

# A ROUTE TO MAGNETIC FIELD REVERSALS: AN EXAMPLE OF AN ABC-FORCED NON-LINEAR DYNAMO

O.M. Podvigina<sup>1</sup>

International Institute of Earthquake Prediction Theory  
and Mathematical Geophysics,  
79 bldg. 2, Warshavskoe ave., 113556 Moscow, Russian Federation

Laboratory of General Aerodynamics, Institute of Mechanics,  
Lomonosov Moscow State University,  
1, Michurinsky ave., 119899 Moscow, Russian Federation

Observatoire de la Côte d'Azur, CNRS UMR 6529,  
BP 4229, 06304 Nice Cedex 4, France

Submitted to *Geophysical & Astrophysical Fluid Dynamics*  
24 July 2002

## Abstract

We are investigating numerically the non-linear behavior of a space-periodic MHD system with ABC forcing. Most computations are performed for magnetic Reynolds numbers increasing from 0 to 60 and a fixed kinematic Reynolds number, small enough for the trivial solution with a zero magnetic field to be stable to velocity perturbations. At the critical magnetic Reynolds number for the onset of instability of the trivial solution the dominant eigenvalue of the kinematic dynamo problem is real. In agreement with the bifurcation theory new steady states with non-vanishing magnetic field appear in this bifurcation. Subsequent bifurcations are investigated. A regime is detected, where chaotic variations of the magnetic field orientation (analogous to magnetic field reversals) are observed in the temporal evolution of the system.

**Key words:** nonlinear magnetic dynamo, bifurcations, reversals

---

<sup>1</sup>E-mail: olgap@mitp.ru

# 1 Introduction

In numerical modelling of physical phenomena two approaches are feasible. On the one hand, one can develop a model as detailed, as possible. Then an obvious difficulty is encountered: usually simplifications are necessary owing to complexity of natural phenomena and/or lack of precise data. Nevertheless, if the model is accurate enough, it displays behavior similar to that of the underlying physical system, when fixed parameter values equal or close to those in the original system are employed. On the other hand, one can consider a class of approximate models, reflecting only global features of the underlying physical system. Parameter values are varied in order to study how this affects the overall behavior of the system. The second approach is advantageous in that properties characterizing the class of systems are revealed; computationally it is usually less demanding, than the first one.

We follow the second approach to acquire information about the succession of temporal regimes which can occur in magnetohydrodynamic (MHD) systems, when Reynolds numbers are increased. In particular, we are concerned with two questions: Which features of MHD systems are responsible for magnetic field reversals – an attribute of the Earth’s magnetic field? Which sequences of bifurcations can bring an MHD system to such a regime?

Reversals were observed in simulations of MHD systems with the geometry and boundary conditions corresponding to those of the Earth (e.g., see Glatzmaier and Roberts, 1995; Sarson and Jones, 1999). However, the computations are very demanding in CPU time, prohibiting numerical identification of complex bifurcations in such systems. Low-dimensional ODE dynamo models, from the one suggested by Rikitake (1958) to those constructed employing central manifold reduction and symmetry considerations (such as Armbruster *et al.*, 2001; Melbourne *et al.*, 2001), can also exhibit reversals. In this paper we consider a system with truncation at fairly large wavenumbers, the resultant system being high-dimensional; space-periodicity assumed here allows to explore a rather wide range of parameters.

Equations of magnetohydrodynamics are invariant under the symmetry, which preserves flows  $\mathbf{v}$  and changes orientation of magnetic fields  $\mathbf{b}$ :

$$h : (\mathbf{v}, \mathbf{b}) \rightarrow (\mathbf{v}, -\mathbf{b}). \tag{1}$$

One can anticipate the following scenario of development of a temporal regime involving magnetic field reversals. Suppose for certain values of a control parameter the system possesses a stable steady state, in which magnetic field vanishes. When the parameter is varied beyond the critical value, two steady states with a non-vanishing magnetic field emerge in a pitchfork bifurcation (generic to systems with the symmetry (1)). In subsequent bifurcations the steady states bifurcate into more complex attractors, related by (1) and remaining so far distinct.

As the parameter is further varied, the attractors of the system join (e.g., due to collision of attractors, or via heteroclinic connection) and a unique

attractor emerges. A sample trajectory on the attractor jumps between former attractors (which degenerate into unstable invariant sets). Since the jumps involve changes in the magnetic field orientation, the resulting intermittency can thus be linked with the reversals.

We consider the Navier-Stokes equation

$$\frac{\partial \mathbf{v}}{\partial t} = \mathbf{v} \times (\nabla \times \mathbf{v}) + \frac{1}{R} \Delta \mathbf{v} - \mathbf{b} \times (\nabla \times \mathbf{b}) + \mathbf{f} - \nabla p \quad (2.a)$$

and the magnetic induction equation

$$\frac{\partial \mathbf{b}}{\partial t} = \nabla \times (\mathbf{v} \times \mathbf{b}) + \frac{1}{R_m} \Delta \mathbf{b} \quad (2.b)$$

under the solenoidality conditions

$$\nabla \cdot \mathbf{v} = 0, \quad \nabla \cdot \mathbf{b} = 0. \quad (2.c)$$

Here  $\mathbf{v}$  is flow velocity,  $\mathbf{b}$  – magnetic field,  $p$  – pressure,  $R$  and  $R_m$  are kinematic and magnetic Reynolds numbers. (Since in the problem under consideration characteristic length and velocity magnitudes are of the order of unity, the Reynolds numbers are defined as inverse viscosity and inverse magnetic diffusivity, respectively.) The fields are supposed to be  $2\pi$ -periodic in space.

The force

$$\mathbf{f} = \mathbf{u}_0 / R \quad (3)$$

is assumed, where  $\mathbf{u}_0$  is an ABC flow

$$\mathbf{u}_0 = (A \sin x_3 + C \cos x_2, B \sin x_1 + A \cos x_3, C \sin x_2 + B \cos x_1). \quad (4)$$

For this force,

$$\mathbf{v} = \mathbf{u}_0, \quad \mathbf{b} = 0 \quad (5)$$

is a steady solution to (2)-(4) for all Reynolds numbers.

This particular system is considered for the following reasons: First, space periodicity enables one to use pseudo-spectral methods (see Canuto *et al.*, 1989; Boyd, 1989), which are computationally efficient. Second, linear stability of the system (2)-(5) to hydrodynamic (Galloway and Frisch, 1987; Podvigina and Pouquet, 1994; Podvigina, 1999) and magnetic (Arnold and Korkina, 1983; Galloway and Frisch, 1986; Galanti *et al.*, 1992; Childress and Gilbert, 1995) perturbations has been investigated both numerically and analytically (nonlinear regimes for some parameter values were also explored by Podvigina and Pouquet, 1994; Podvigina, 1999; Galanti *et al.*, 1992; Feudel *et al.*, 1996; Brummel *et al.*, 2001). These studies provide guidance, in what parameter ranges the targeted type of behavior may be observed. In particular, growing magnetic modes exist for the flow (3) in broad intervals of constants  $A$ ,  $B$  and  $C$ . Third, since the critical magnetic Reynolds number is typically of the order of 10, only moderate  $R_m$  need to be considered, and a relatively low resolution ( $32^3$  Fourier harmonics) suffices.

Magnetic field growth rates were calculated by Galanti *et al.* (1992) for the flow (4) with the coefficients satisfying  $B = C$ ,  $A^2 + B^2 + C^2 = 3$ ,  $0 < B/A < 1$  for various values of  $R_m$ . For  $R_m = 12$  there are three windows in  $B/A$  of positive growth rates (see Fig. 2 *ibid.*). We have checked that in the window  $0.7 < B/A < 0.9$  the dominant eigenvalue is real, and in the other two windows it is complex. Distinct steady states with a non-zero magnetic field appear in a bifurcation of the trivial steady state (5), only if the magnetic induction operator has a zero (hence real) eigenvalue at the bifurcation point. This has suggested to set

$$A = 1, \quad B = C = 0.75; \quad (6)$$

these values of constants in (4) are assumed throughout.

In the present study we focus at non-hydrodynamic attractors. The hydrodynamic global stability of  $\mathbf{u}_0$  guarantees that magnetic field does not vanish in saturated regime, if  $\mathbf{v} = \mathbf{u}_0$  is a kinematic dynamo. We have verified that for  $R = 4$ ,  $\mathbf{v} = \mathbf{u}_0$  is a unique attractor of the hydrodynamic system ( (2.a,2.c) with  $\mathbf{b} = 0$ ), and most computations are made for this value of  $R$ . Several runs are also performed for higher  $R$ .

A perturbation of the trivial steady state (5) with the energy of  $10^{-6}$  in each Fourier harmonics spherical shell is employed as an initial condition. The range of existence of attractors is determined by continuation in parameter: the runs are done with an initial condition, which is a point on the attractor for close values of  $R_m$ .

## 2 Symmetries

The group of symmetries without inversion of time of an ABC flow with  $B = C$ ,  $\mathcal{G}$ , is comprised of two independent symmetries

$$s_1 : x_1 \rightarrow -\frac{\pi}{2} - x_3, \quad x_2 \rightarrow -\frac{\pi}{2} - x_2, \quad x_3 \rightarrow -\frac{\pi}{2} - x_1,$$

$$s_2 : x_1 \rightarrow \frac{\pi}{2} + x_3, \quad x_2 \rightarrow -\frac{\pi}{2} + x_2, \quad x_3 \rightarrow \frac{\pi}{2} - x_1,$$

their superpositions

$$s_3 = s_2^2 : x_1 \rightarrow \pi - x_1, \quad x_2 \rightarrow \pi + x_2, \quad x_3 \rightarrow -x_3,$$

$$s_4 = s_2^3 : x_1 \rightarrow \frac{\pi}{2} - x_3, \quad x_2 \rightarrow \frac{\pi}{2} + x_2, \quad x_3 \rightarrow -\frac{\pi}{2} + x_1,$$

$$s_5 = s_1 s_2 : x_1 \rightarrow \pi + x_1, \quad x_2 \rightarrow -x_2, \quad x_3 \rightarrow \pi - x_3,$$

$$s_6 = s_1 s_2^2 : x_1 \rightarrow -\frac{\pi}{2} + x_3, \quad x_2 \rightarrow \frac{\pi}{2} - x_2, \quad x_3 \rightarrow \frac{\pi}{2} + x_1$$

$$s_7 = s_1 s_2^3 : x_1 \rightarrow -x_1, \quad x_2 \rightarrow \pi - x_2, \quad x_3 \rightarrow \pi + x_3,$$

and the identity transformation  $s_8 = e$  (Arnold, 1984; Dombre *et al.*, 1986; Podvigina and Pouquet, 1994). The group is isomorphic to the symmetry group of a square,  $\mathbf{D}_4$ .

Any symmetry of the force (3),(4) which does not involve inversion of time is also a symmetry of the Navier-Stokes equation (2.a) with  $\mathbf{b} = 0$ . The group of symmetries of the MHD system (2)-(4),(6) is a direct product of  $\mathcal{G}$  and the 2-element group  $\mathbf{Z}_2$ , generated by  $h$  (1). It has 16 elements, which are either  $s_i$  or  $hs_i$ .

Let  $\mathcal{A}$  be an attractor of a dynamical system, invariant under a symmetry  $g$ :  $g(\mathcal{A}) = \mathcal{A}$ . Two cases can be distinguished: either  $\mathcal{A}$  is pointwise invariant, i.e.  $g(\mathbf{x}) = \mathbf{x}$  for all points  $\mathbf{x} \in \mathcal{A}$ , or it is invariant only as a set, with  $g(\mathbf{x}) \neq \mathbf{x}$  for some  $\mathbf{x} \in \mathcal{A}$ . In what follows, only the symmetries for which an attractor is pointwise invariant are regarded as symmetries of the attractor.

### 3 Attractors of the MHD system for $R = 4$

Results of computations are summarized in Table 1. For  $15 \leq R_m \leq 58$  the system under consideration possesses multiple attractors. For  $16 \leq R_m \leq 58$  attractors, which we have detected, belong to two independent families; within each family they are genetically related by sequences of bifurcations. Attractors from different families have distinct groups of symmetries. The families can be distinguished also by their time-averaged kinetic ( $\overline{E}_k$ ) and magnetic ( $\overline{E}_m$ ) energies:  $0.9 < \overline{E}_k < 1.1$ ,  $0 \leq \overline{E}_m < 0.05$  for the first family, and  $0.3 < \overline{E}_k < 0.7$ ,  $0.07 < \overline{E}_m < 0.25$  for the second one.

The first family exists for  $0 \leq R_m \leq 58$ : the first attractor is the trivial steady state (5) (denoted by  $S_0$ ) remaining stable up to<sup>2</sup>  $R_m = 14$ . It becomes unstable in a pitchfork bifurcation, in which two stable mutually symmetric steady states ( $S_{1,1}$  and  $S_{1,2}$ ) with a non-zero magnetic field emerge. The 8-element symmetry group of  $S_{1,i}$  is isomorphic to  $\mathbf{D}_4$ ; however, it is distinct from  $\mathcal{G}$ .

The second family emerges between  $R_m = 15$  and  $R_m = 16$ : in addition to the steady states  $S_{1,i}$ , for  $R_m \geq 16$  the system possesses another attractor, a stable periodic orbit  $P_1$ . The orbit does not exist for  $R_m \leq 15$ ; apparently it appears in a saddlenode bifurcation. For  $R_m = 26$  the orbit is unstable and a torus  $T_1$  has appeared in a Hopf bifurcation.  $T_1$  remains an attractor for all higher considered  $R_m$  (specifically, for  $R_m = 26, 27, 30, 40, 57$  and 60). For  $R_m \geq 57$  the torus attracts trajectories (in the phase space) initially close to the trivial steady state  $S_0$ , and for  $R_m \geq 59$  it is the only global attractor of the system. The torus  $T_1$  and the orbit  $P_1$  were traced back from  $R_m = 57$  by continuation in  $R_m$ . In what follows we will not discuss this family of attractors any more.

The steady states  $S_{1,i}$  become unstable in a supercritical Hopf bifurcation at the interval  $24 < R_m < 25$ . A stable periodic orbit  $P_{2,i}$  of period  $\approx 12$

---

<sup>2</sup>This is consistent with results of Galanti *et al.* (1992): since the ABC coefficients (6) are not normalized to satisfy  $A^2 + B^2 + C^2 = 3$  as they were in the cited paper, Reynolds numbers referred to here are lower by a factor  $(17/24)^{1/2}$ .

Table 1. Attractors, detected for the MHD system with the forcing (3), (4), (6) for  $R = 4$  and  $0 \leq R_m \leq 60$ . The third column shows the number of elements of the symmetry group for which an attractor is pointwise invariant, and the fourth column – generators of the group. Indices in the labels of attractors (second column) have the following meaning. For periodic orbits emerging in the period doubling cascade the superscript  $M$  refers to an  $M\tau$ -period orbit,  $\tau$  being the period of the foremost orbit. The first subscript labels different attractors of a given kind. The second subscript labels mutually symmetric attractors.

$R_m$	Attractors	Number of symmetries	Generators
$R_m \leq 14$	steady state $S_0$	16	$s_1, s_2, h$
$15 \leq R_m \leq 24$	steady states $S_{1,i}$ ( $i = 1, 2$ )	8	$hs_1, s_2$
$25 \leq R_m \leq 37$	periodic orbits $P_{2,i}$ ( $i = 1, 2$ )	4	$hs_1, s_3 (= s_2^2)$
$37.5 \leq R_m \leq 38.5$	steady states $S_{1,i}$ ( $i = 1, 2$ )	8	$hs_1, s_2$
$39 \leq R_m \leq 39.2$	periodic orbits $P_{3,i}^1$ ( $i = 1, 2$ )	8	$hs_1, s_2$
$39.3 \leq R_m \leq 39.4$	periodic orbits $P_{3,i}^2$ ( $i = 1, 2$ )	8	$hs_1, s_2$
$R_m = 39.45$	periodic orbits $P_{3,i}^4$ ( $i = 1, 2$ )	8	$hs_1, s_2$
$R_m = 39.5$	chaotic $C_{1,i} = P_{3,i}^\infty$ ( $i = 1, 2$ )	8	$hs_1, s_2$
$R_m = 39.6$	periodic orbits $P_{3,i}^1$ ( $i = 1, 2$ ) & periodic orbit $P_4$	8 8	$hs_1, s_2$ $hs_1, s_2$
$39.7 \leq R_m \leq 41$	periodic orbit $P_4$	8	$hs_1, s_2$
$R_m = 42, 43$	tori $T_{2,i}$ ( $i = 1, 2$ )	4	$hs_1, s_3$
$R_m = 45$	chaotic $C_{2,i}$ ( $i = 1, 2$ )	4	$hs_1, s_3$
$R_m = 46, 47$	chaotic $C_{3,i}$ ( $i = 1, 4$ )	2	$hs_1$
$R_m = 48, 49$	chaotic $C_{4,i}$ ( $i = 1, 4$ )	2	$hs_1$
$R_m = 50, 51$	chaotic $C_{5,i}$ ( $i = 1, 2$ )	2	$hs_1$
$52 \leq R_m \leq 58$	tori $T_{3,i}$ ( $i = 1, 4$ )	2	$hs_1$
$16 \leq R_m \leq 25$	periodic orbit $P_1$	4	$hs_2$
$26 \leq R_m \leq 60$	torus $T_1$	4	$hs_2$

appears in a vicinity of the steady state  $S_{1,i}$ . The two orbits are mutually symmetric (they are interrelated by (1)). Each periodic orbit possesses all 8 symmetries of its parent steady state, but each individual point of the orbit has a symmetry group of only 4 elements (it is isomorphic to  $\mathbf{D}_2$ ). The orbits exist for  $25 \leq R_m \leq 37$  remaining attracting. A typical behavior of a trajectory is shown on Fig. 1 for  $R_m = 30$ . After an initially small magnetic energy at first exponentially grows and afterwards decays with oscillations, it subsequently levels off (see a plateau about 400 time units long on Fig. 1a): the trajectory in the phase space evolves in a vicinity of  $S_{1,i}$  (which is unstable now). In the further evolution the trajectory leaves the steady state, being attracted by  $P_{2,i}$  (see Fig. 1b). The orbits disappear in a subcritical Hopf bifurcation between  $R_m = 37$  and  $R_m = 37.5$ . For  $R_m = 37.5, 38$  and  $38.5$  the two steady states  $S_{1,i}$  are verified to be stable.

Next bifurcation of  $S_{1,i}$  is again a supercritical Hopf bifurcation. The emerging mutually symmetric periodic orbits  $P_{3,i}^1$ ,  $i = 1, 2$  (one for each of the two steady states) possess all the symmetries of the steady states. For  $39 \leq R_m \leq 39.2$  they are attracting, and their period is  $\tau(P_{3,i}^1) \approx 120$ . Behavior of a sample trajectory in the phase space (see Fig. 2) resembles the one shown on Fig. 1; however, on Fig. 2a the plateau corresponding to the evolution in the vicinity of the unstable steady state  $S_{1,i}$  virtually disappears, and the period is much larger. The orbit is located in a different region of the phase space (cf. Fig. 1b and Fig. 2b). At an  $R_m$  between 39.2 and 39.3 two mutually symmetric orbits  $P_{3,i}^2$  ( $i = 1, 2$ ) of a twice larger period emerge (see Fig. 3a). A sequence of period-doubling bifurcations begins. The next period doubling occurs at the interval  $39.4 < R_m < 39.45$  (see period-four orbit  $P_{3,i}^4$  for  $R_m = 39.45$  on Fig. 3b). At  $R_m = 39.5$  a trajectory, initially close to  $S_0$ , is either already chaotic, or close to an orbit of a very long period  $P_{3,i}^\infty$  (see Fig. 3c). This indicates that at  $R_m = 39.5$  the period-doubling cascade is over. For  $R_m = 39.6$  a trajectory with the same initial condition is attracted to a period-one orbit  $P_{3,i}^1$ .

Another attractor exists for  $R_m = 39.6$ . It reveals itself when the attractor for  $R_m = 39.7$ , which is unique in this region of the phase space (see below) is continued in smaller  $R_m$ . This is a periodic orbit  $P_4$ , involving transitions between the two period-two orbits  $P_{3,1}^2$  and  $P_{3,2}^2$  (see Fig. 4a). The orbit is invariant under  $h$  (1) and any symmetry from  $\mathcal{G}$ . In the course of temporal evolution, direction of magnetic field is reversed, behavior of non-zero magnetic field Fourier coefficients is similar to that shown on Fig. 4b. A reversal takes a relatively short time, during which initially the energy of magnetic field attains the minimum and kinetic – the maximum, and subsequently magnetic energy blows up to a maximum, with the kinetic energy simultaneously reaching its minimum (Fig. 4c,d). No attractor of this type is revealed by further continuation in smaller  $R_m$ .

This bifurcation is apparently of the following nature. In the period-doubling cascade infinitely many unstable periodic orbits  $P_{3,i}^M$  ( $i = 1, 2$ ) of

periods  $\tau(P_{3,i}^M) = M\tau(P_{3,i}^1)$  are created. Consider two such orbits  $P_{3,i}^m$  ( $m = 2$  in our case) related by (1). Suppose that for some value of a control parameter the stable manifold of  $P_{3,1}^m$  intersects the unstable manifold of  $P_{3,2}^m$ , and a heteroclinic trajectory connecting these orbits emerges. Consider the symmetry, which maps one of the periodic orbits to another. Under this symmetry the heteroclinic trajectory is mapped to a distinct heteroclinic trajectory, and the two form a heteroclinic cycle. The cycle may give rise to a periodic orbit  $P_4$ , when the control parameter varies. (This scenario is analogous to that in two-dimensional dynamical systems, where a homoclinic connection generically implies for close values of the control parameter existence of periodic orbits in a vicinity of the homoclinic trajectory, and their period tends to infinity when the critical value is approached.)

For  $39.7 \leq R_m \leq 41$  sample trajectories, initially close to the trivial steady state  $S_0$ , are attracted by the periodic orbit  $P_4$ . However, while for  $R_m = 39.6$  such a trajectory follows closely each of  $P_{3,i}^2$  (Fig. 4a), this is not the case any more for higher  $R_m$  (see Fig. 5). In agreement with our conjecture that appearance of the orbit is related to heteroclinic connection, the period decreases from 800 for  $R_m = 39.7$  to 500 for  $R_m = 41$ .

For  $R_m = 42$  and  $43$  the regime is quasi-periodic: the orbit  $P_4$  bifurcates into two attracting tori  $T_{2,i}$  ( $i = 1, 2$ ) interrelated by (1) (see Fig. 6). The second frequency can be observed on Fig. 6a, showing real part of the Fourier component  $b_{0,1,1}^3$  of magnetic field. The time average of this Fourier component is negative (Fig. 6a); hence, the symmetry (1) maps this attractor to a distinct one. (For  $37.5 \leq R_m \leq 41$  the component vanishes, because former attractors [ $P_4$  for  $39.6 \leq R_m \leq 41$ ,  $P_{3,i}^m$  for  $39 \leq R_m \leq 39.6$ , and  $S_{1,i}$  for  $37.5 \leq R_m \leq 38.5$ ] possess the symmetry  $hs_5 = hs_1s_2$ .) Note qualitatively different behavior (Figs. 6a and 6b) of different Fourier coefficients of the magnetic field (for  $R_m \leq 41$  all non-zero components evolved coherently).

For  $R_m = 45$  two mutually symmetric attractors persist (Fig. 7): each torus  $T_{2,i}$  bifurcates into a chaotic attractor  $C_{2,i}$ . Reversals are less regular, yet they are too ordered in comparison with those of the Earth's magnetic field.

For  $R_m = 46$  (Fig. 8) behavior of a sample trajectory suggests existence of four (unstable) steady states  $S_{2,i}$  (see plateaux at  $1500 \leq t \leq 2100$ ). They are mutually symmetric, and have the same 4-element symmetry group generated by  $hs_1$  and  $s_3$ . Apparently two  $S_{2,i}$ 's emerged from each  $S_{1,i}$  in a pitchfork bifurcation. Initially (at  $0 \leq t < 700$ ) the sample trajectory for  $R_m = 46$  undergoes several reversals, similar in nature to those observed for  $39.7 \leq R_m \leq 45$ . Afterwards it is attracted to a steady state  $S_{2,i}$ . Subsequent sample evolution consists of transitions between the steady state  $S_{2,i}$  and the region of the phase space where a former chaotic attractor  $C_{2,i}$  was located (duration of repeating events in the saturated regime is  $\approx 1700$ ). In particular, large-amplitude excursions at  $2350 \leq t \leq 2500$ ,  $2300 \leq t \leq 2450$ ,  $4000 \leq t \leq 4150$ , etc., are reminiscent of the behavior of a  $C_{2,i}$  trajectory for  $R_m = 45$ . Thus, apparently two former chaotic attractors  $C_{2,i}$  have disappeared in collision with the four

steady states  $S_{2,i}$  to give rise to four new chaotic attractors  $C_{3,i}$ . It is notable that the sample trajectory leaves a vicinity of the  $S_{2,i}$  in alternating directions along the unstable manifold. For  $R_m = 47$  the behavior is similar to the one at  $R_m = 46$ .

For  $R_m = 48$  the system possesses four mutually symmetric attractors  $C_{4,i}$ . Events are longer than in the previous regime, about 3000 time units (see Fig. 9). They exhibit a new feature, a phase of initially exponentially decaying oscillations (e.g. at  $1700 \leq t \leq 2300$  and  $4500 \leq t \leq 5200$ ). This indicates existence of a weakly unstable periodic orbit of a new kind,  $P_{5,i}$  ( $i = 1, 4$ ), in a vicinity of the former chaotic attractor  $C_{3,i}$ . A similar behavior is also observed for  $R_m = 49$ .

For  $R_m = 50, 51$  (Fig. 10) the four  $C_{4,i}$  are superceded by two new attractors,  $C_{5,i}$ . Large amplitude oscillations, e.g. at  $7500 \leq t \leq 8500$ , are due to attraction of the trajectory by weakly unstable tori  $T_{3,i}$  ( $i = 1, 4$ ), which have bifurcated from the periodic orbits  $P_{5,i}$ . In the saturated regime behavior consists of three phases: (i) a trajectory is close to a periodic orbit  $P_{5,i}$  (e.g. at  $2300 \leq t \leq 3000$  and  $4300 \leq t \leq 5000$ ); (ii) the trajectory evolves in the vicinity of a torus  $T_{3,i}$  (e.g. at  $3200 \leq t \leq 4000$  and  $5300 \leq t \leq 6000$ ); (iii) the trajectory abruptly jumps toward the second periodic orbit  $P_{5,i'}$  to reproduce the sequence of phases.

For  $R_m = 52$  each of the two former chaotic attractors splits into two attracting tori  $T_{3,i}$  (Fig. 11; cf. Figs. 10b and 11b). The four new attractors are mutually symmetric, they are stable for  $52 \leq R_m \leq 58$ .

For  $57 \leq R_m \leq 60$  a sample trajectory initially close to  $S_0$  is attracted by the torus  $T_1$ .

## 4 Attractors of the MHD system for $R_m = 40$ .

Simulations are performed for  $R_m = 40$  and for several values of  $R$  with an initial condition, same for all runs, being a small perturbation of  $S_0$  (see Table 2). The question we address is how the temporal behavior changes with  $R$ , in particular, if for higher  $R$  reversals persist, or whether magnetic field vanishes in a saturated regime. (If (2) possesses attractors with  $\mathbf{b} = 0$  different from the trivial steady state, an initially growing magnetic field can die out in the nonlinear regime, the resulting attractor being purely hydrodynamical, see Brummel *et al.*, 1998; Matthews, 2000.) Computations with the same  $R$  and the same initial condition for the flow are also performed for the purely hydrodynamic system (2.a), in order to compare the behavior and attractors of the two systems.

For  $R = 3$  the detected attractor is the torus  $T_1$  (which is an attractor for  $R = 4$  and  $26 \leq R_m \leq 60$ ). For  $R = 6$  reversals take place, similar to those observed for  $R = 4$  and  $R_m = 45$ , and the attractor is  $C_{2,i}$ . Thus, for  $R$  close to 4 no new attractors are found.

Table 2. Attractors, detected for the MHD system with the force (3), (4), (6) for  $R_m = 40$  and  $3 \leq R \leq 25$ . The third column shows the number of elements of the symmetry group for which an attractor is pointwise invariant, and the fourth – generators of the group.

$R$	Attractors	Number of symmetries	Generators	$\overline{E}_k$	$\overline{E}_m$
$R = 3$	$T_1$	4	$hs_2$	0.4	0.25
$R = 4$	chaotic $P_4$	8	$hs_1, s_2$	0.95	0.03
$R = 6$	chaotic $C_{2,i}$ ( $i = 1, 2$ )	4	$hs_1, s_3$	0.95	0.03
$R = 10$	periodic orbit $P_6$	8	$hs_1, s_2$	0.5	0.06
$R = 15$	chaotic $C_6$	4	$s_1, s_3$	0.6	0.04
$R = 20$	tori $T_{4,i}$ ( $i = 1, 2$ )	4	$s_1, s_3$	0.7	0.01
$R = 25$	chaotic $C_{7,i}$ ( $i = 1, 2$ )	1	$e$	0.5	0.02

Table 3. Attractors, detected for the hydrodynamic system (2.a) with the force (3), (4), (6) for  $3 \leq R \leq 25$ . The third column shows the number of elements of the symmetry group for which an attractor is pointwise invariant, and the fourth column – generators of the group.

$R$	Attractors	Number of symmetries	Generators	$\overline{E}_k$
$R = 3, 4, 6$	$\mathbf{u}_{ABC}$	8	$s_1, s_2$	1.06
$R = 10^*$	$\mathbf{u}_{ABC}$	8	$s_1, s_2$	1.06
	$S_1^h$	8	$s_1, s_2$	0.99
$R = 15$	$S_1^h$	8	$s_1, s_2$	0.93
$R = 20$	chaotic $C_1^h$	4	$s_2$	0.9
$R = 25$	chaotic $C_2^h$	1	$e$	0.7

\*  $S_1^h$  for  $R = 10$  was traced back from  $R = 15$ ; it is not observed for  $R = 6$ .

For  $R = 10$  a new attractor was found in the full MHD system – a periodic orbit  $P_6$  with a symmetry group of 8 elements. Comparison of Tables 2 and 3 reveals no relation of attractors of the hydrodynamic and MHD systems for  $R = 10, 15$  and  $20$ . For these Reynolds numbers a small magnetic field (magnetic energy  $E_m$  is below 0.07; see Table 2) drastically changes behavior of the system – the hydrodynamic and MHD systems have attractors of different types, and the average kinetic energy  $\overline{E}_k$  decreases significantly, e.g. for  $R = 20$   $\overline{E}_m = 0.01$  and  $\overline{E}_k$  decreases from 0.9 (the hydrodynamic case) to 0.7 (the MHD case).

For  $R = 15$  behavior of the sample trajectory of the MHD system in saturated regime is chaotic. But before the saturated regime sets in, the trajectory is attracted by  $P_6$  and for  $1000 \leq t \leq 2000$  remains close to this periodic orbit (see Fig. 12), which is now weakly unstable. For  $R = 20$  the trajectory with the same initial condition is attracted to a new torus  $T_{4,i}$ ; initially the temporal behavior of the trajectory resembles the one observed for  $R = 15$  (cf. Figs. 12 and 13).

For  $R = 25$  the MHD system possesses new chaotic attractors  $C_{7,i}$  ( $i = 1, 2$ ) with a trivial symmetry group. They resemble the chaotic attractor  $C_6$  observed for  $R = 15$  (cf. Fig. 12 and Fig. 14), but unlike  $C_{7,i}$ ,  $C_6$  is unique and has a symmetry group of four elements. Comparison of  $C_{7,i}$  with the attractor of the non-magnetic Navier-Stokes equation, which also is chaotic, reveals that the influence of magnetic field is in some sense stabilizing: Fourier coefficients of the flow experience fewer jumps and the amplitude of their oscillations is much smaller (compare Fourier components of flows on Figs. 14b and 15b). An exponential growth of the initially small magnetic field in the sample evolution of the system begins only at  $t = 200$  (Fig. 14c). Accordingly, until  $t = 300$  the flow evolution is similar to the one in the absence of magnetic field. Magnetic field starts growing, when the trajectory is attracted by a weakly unstable periodic orbit in the hydrodynamic subspace. Departure from this orbit causes an initial decay of magnetic field before the onset of saturated behavior.

For  $R = 15$  and  $20$  behavior of Fourier components of magnetic field is similar to the one shown on Fig. 14d. It consists of chaotic irregular small-period oscillations about zero, different from the behavior observed for  $R = 4$ . Thus for  $R_m = 40$ ,  $15 \leq R \leq 25$  the considered system is not in a regime resembling reversals.

## 5 Conclusion

Our computations show that irregular magnetic field reversals are an inherent feature of a nonlinear dynamical system of an MHD type. The simulated reversals appear more regular than those of the Earth, since they are observed for much smaller values of Reynold’s numbers. The dissimilarity with reversals of the Earth’s magnetic field also stems from the fact that we consider a simplified set of equations (neither an account of thermal or sedimentation-

driven convection is taken, nor that of the Coriolis force) in an idealized space-periodic geometry. Other types of behavior, all with a non-vanishing magnetic field, are found when any of the Reynolds numbers is increased.

The bifurcation scenario leading to emergence of reversals, which we put forward, proves feasible. Reversals are found only for small  $R$ , for which the hydrodynamic system has a unique globally stable steady state. Complexity of the sequence of bifurcations obtained in simulations is comparable to that of the hydrodynamic system examined by Podvigina and Pouquet (1994) and Podvigina (1999). Numerous types of behavior are identified, which involve a large variety of attractors and unstable invariant sets of various types affecting behavior of evolutionary solutions. Regime of reversals arises as a result of merging of two distinct attractors, apparently via heteroclinic connection due to intersection of stable and unstable manifolds of periodic orbits. This is in contrast with the system studied by Armbruster *et al.* (2001), where a heteroclinic cycle emerged together with magnetic steady states.

### Acknowledgments

I am grateful to V. Zheligovsky for discussions. Part of this research was carried out during my stays at the School of Mathematical Sciences, University of Exeter, UK, in January – February 2001 and in May – July 2002. I am grateful to the Royal Society for their support of the two visits. Some numerical results were obtained using computational facilities provided by the program “Simulations Interactives et Visualisation en Astronomie et Mécanique (SIVAM)” at Observatoire de la Côte d’Azur, France. My research work at Observatoire de la Côte d’Azur was supported by the French Ministry of Education. Part of the work was done during a visit to Departamento de Matemática Aplicada, Faculdade de Ciências, University of Porto, Portugal at the kind invitation of Centro de Matemática Aplicada in June – July, 2001.

### References

- Armbruster, D., Chossat, P., and Oprea, I., Structurally stable heteroclinic cycles and the dynamo dynamics, In: *Dynamo and Dynamics, a Mathematical Challenge* (Eds. Chossat, P., Armbruster, D. and Oprea, I.), pp. 313–322, Kluwer Academic Publishers (2001).
- Arnold V.I. and Korkina E.I. The growth of a magnetic field in a three-dimensional incompressible flow, *Vestnik Moscow State Univ., Ser. Math.* **3**, 43–46 (1983) (in Russian).
- Arnold V.I. On the evolution of magnetic field under the action of advection and diffusion, in *Some problems of modern analysis* (ed. V.M. Tikhomirov). Moscow Univ. Press, 8–21 (1984) (in Russian).
- Boyd J.P. *Chebyshev & Fourier Spectral Methods*. Springer-Verlag, Berlin (1989).

- Brummel N.H., Cattaneo F. and Tobias S.M. Linear and nonlinear dynamo action, *Phys. Lett. A* **28**, 437–442 (1998).
- Brummel N.H., Cattaneo F. and Tobias S.M. Linear and nonlinear dynamo properties of time-dependent ABC flows, *Fluid Dyn. Res.* **28**, 237–265 (2001).
- Canuto C., Hussaini M.Y., Quarteroni A. and Zang T.A. *Spectral Methods in Fluid Dynamics*, Springer-Verlag, Berlin (1988).
- Childress S. and Gilbert A.D. *Stretch, twist, fold: the fast dynamo*. Springer-Verlag, Berlin (1995).
- Dombre T., Frisch U., Greene J.M., Hénon M., Mehr A. and Soward A. Chaotic streamlines in the ABC flows, *J. Fluid Mech.* **167**, 353–391 (1986).
- Feudel S., Seehafer N., Galanti B. and Schmidtman O. Symmetry breaking bifurcation for the magnetohydrodynamic equation with helical forcing, *Phys. Rev. E* **54**, 2589–2596 (1996).
- Galanti B., Sulem P.L. and Pouquet A. Linear and Non-Linear Dynamos Associated With ABC Flows, *Geophys. Astrophys. Fluid Dynamics* **66**, 183–208 (1992).
- Galloway D.J. and Frisch U. Dynamo action in a family of flows with chaotic streamlines, *Geophys. Astrophys. Fluid Dynamics* **36**, 53–83 (1986).
- Galloway D.J. and Frisch U. A note on the stability of a family of space-periodic Beltrami flows, *J. Fluid Mech.* **180**, 557–564 (1987).
- Glatzmaier G.A. and Roberts P.H. A three-dimensional self-consistent computer simulation of a geomagnetic field reversal. *Nature* **377**, 203–209 (1995).
- Matthews, P.C., Dynamo action in simple convective flows, *Proc. R. Soc.* **455**, 1829–1840 (1999).
- Melbourne, I., Proctor, M.R.E. and Rucklidge, A.M., A heteroclinic model of geodynamo reversals and excursions, In: *Dynamo and Dynamics, a Mathematical Challenge* (Eds. Chossat, P., Armbruster, D. and Oprea, I.), pp. 313–322, Kluwer Academic Publishers (2001).
- Podvigina O. and Pouquet A. On the non-linear stability of the 1:1:1 ABC flow, *Physica D* **75**, 471–508 (1994).
- Podvigina O.M. *Spatially-periodic evolutionary and steady solutions to the three-dimensional Navier-Stokes equation with the ABC-force*. Institute of Mechanics, Lomonosov Moscow State University (1999).
- Rikitake, T., Oscillations of a system of disk dynamo, *Proc. Camb. Phil. Soc.* **54**, 89–105 (1958).
- Sarson G.R. and Jones C.A. A convection driven geodynamo reversal model, *Phys. Earth Planet. Int.* **111**, 3–20 (1999).

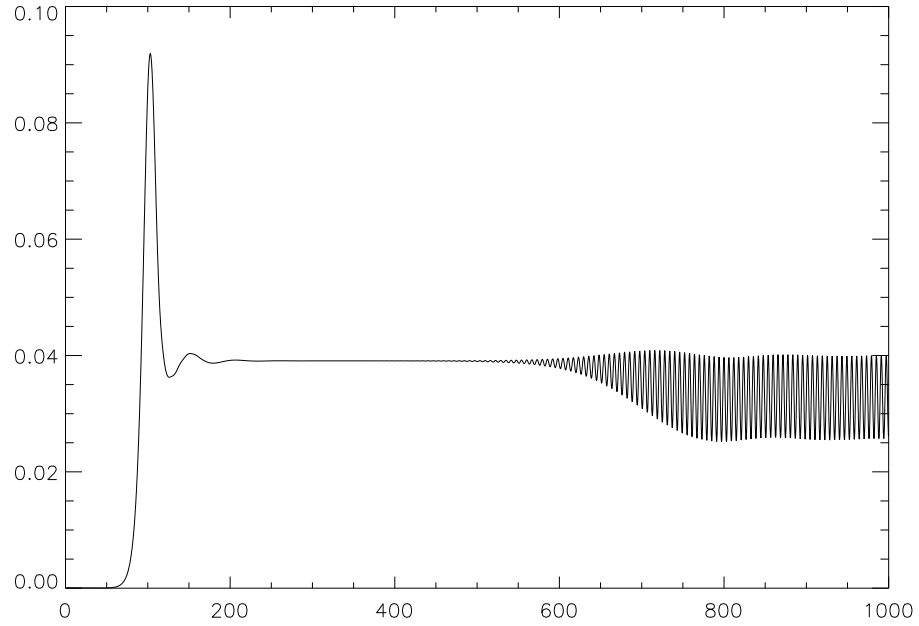


Figure 1a. Magnetic energy (vertical axis) as a function of time (horizontal axis) for  $R = 4$  and  $R_m = 30$ .

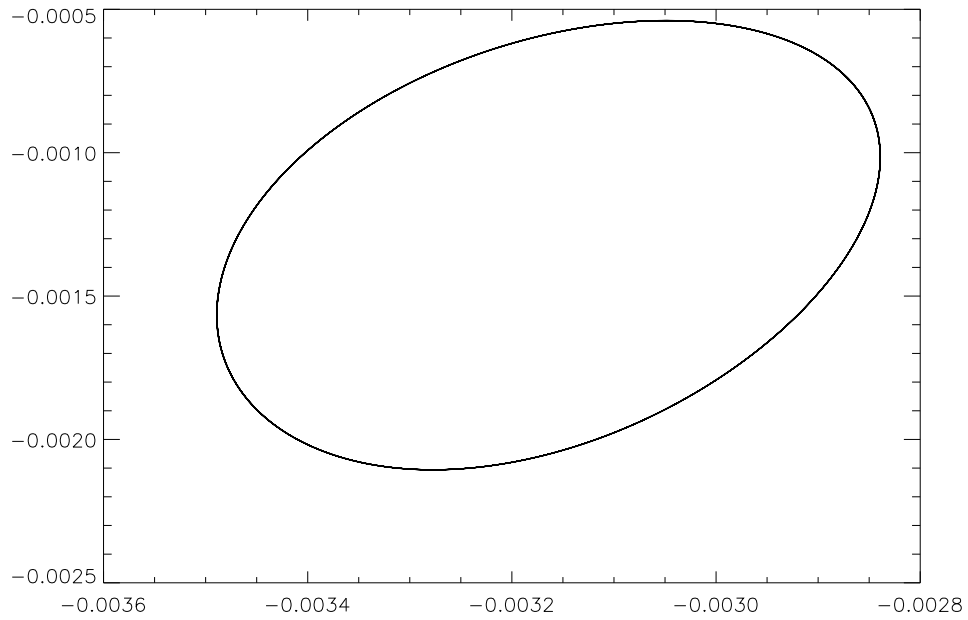


Figure 1b. Projection of the trajectory in saturated regime (a periodic orbit  $P_{2,i}$ ) on the plane of Fourier coefficients  $\text{Im } b_{0,1,2}^1$  (horizontal axis) and  $\text{Re } v_{0,1,2}^1$  (vertical axis) for  $R = 4$  and  $R_m = 30$  (same run as on Fig. 1a).

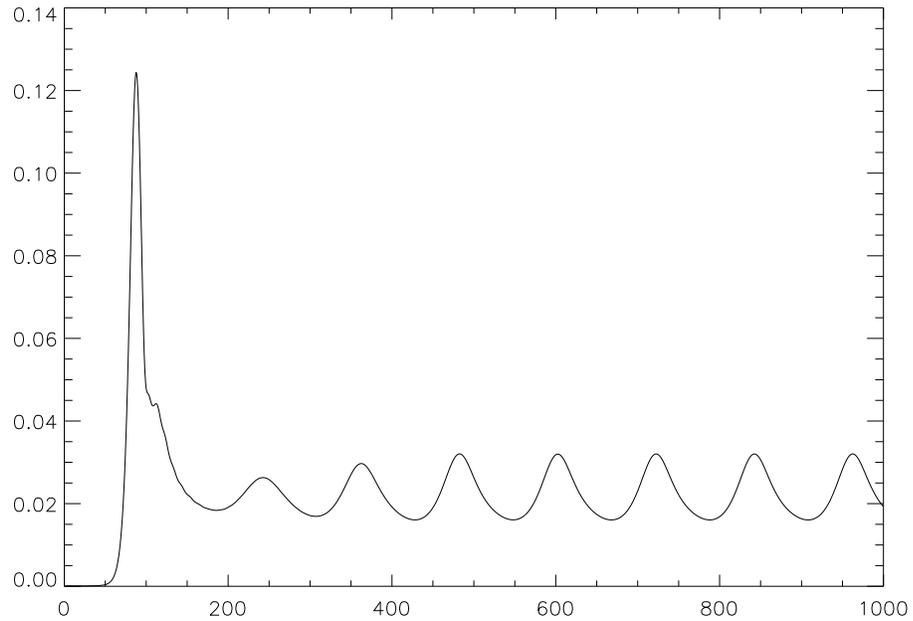


Figure 2a. Magnetic energy (vertical axis) as a function of time (horizontal axis) for  $R = 4$  and  $R_m = 39.2$ .

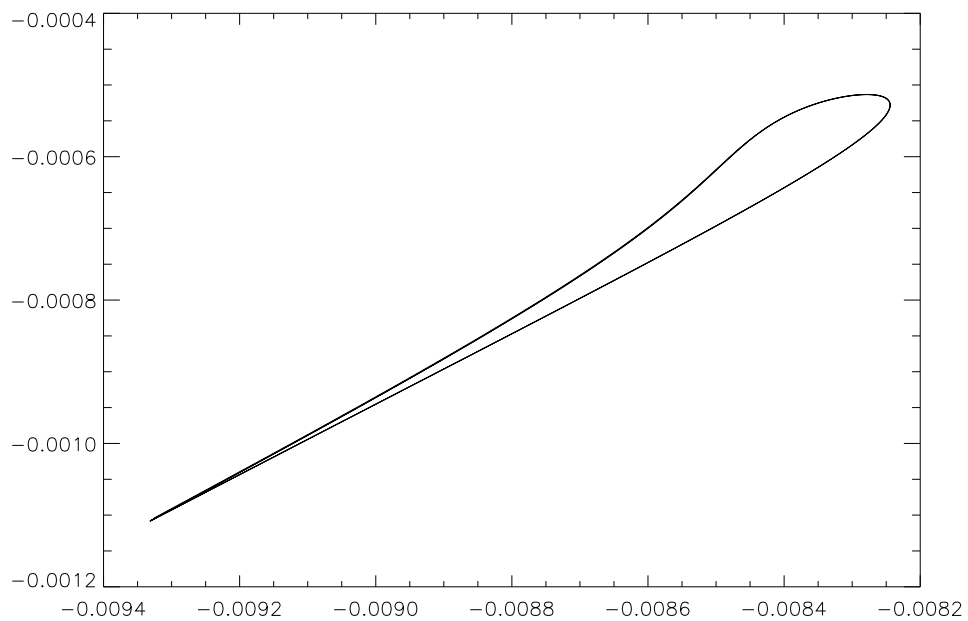


Figure 2b. Projection of the trajectory in saturated regime (a periodic orbit  $P_{3,i}^1$ ) on the plane of Fourier coefficients  $\text{Im } b_{0,1,2}^1$  (horizontal axis) and  $\text{Re } v_{0,1,2}^1$  (vertical axis) for  $R = 4$  and  $R_m = 39.2$  (same run as on Fig. 2a).

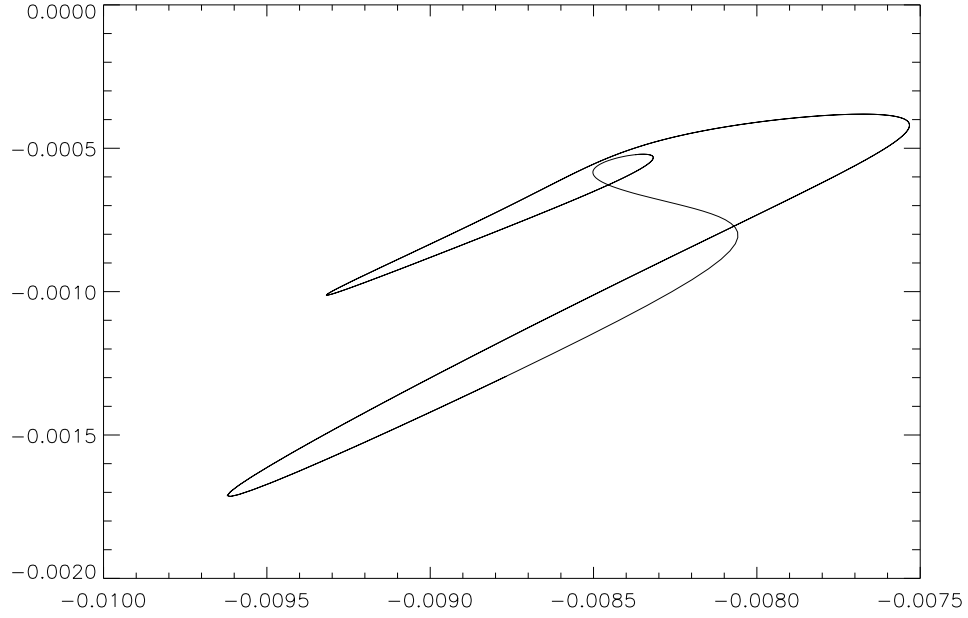


Figure 3a. Projection of the trajectory in saturated regime (a periodic orbit  $P_{3,i}^2$ ) on the plane of Fourier coefficients  $\text{Im } b_{0,1,2}^1$  (horizontal axis) and  $\text{Re } v_{0,1,2}^1$  (vertical axis) for  $R = 4$  and  $R_m = 39.4$ .

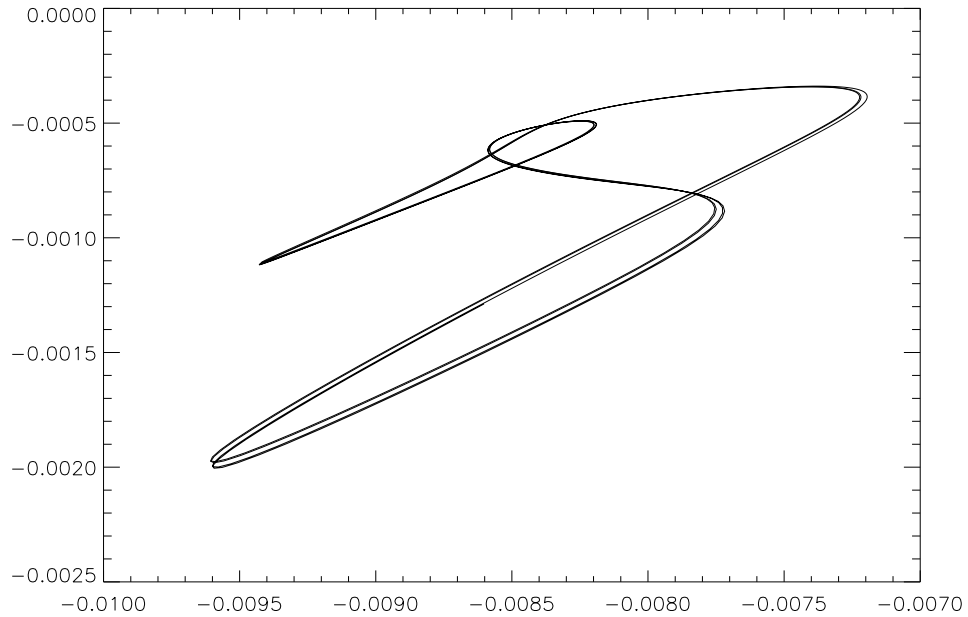


Figure 3b. Projection of the trajectory in saturated regime (a periodic orbit  $P_{3,i}^4$ ) on the plane of Fourier coefficients  $\text{Im } b_{0,1,2}^1$  (horizontal axis) and  $\text{Re } v_{0,1,2}^1$  (vertical axis) for  $R = 4$  and  $R_m = 39.45$ .

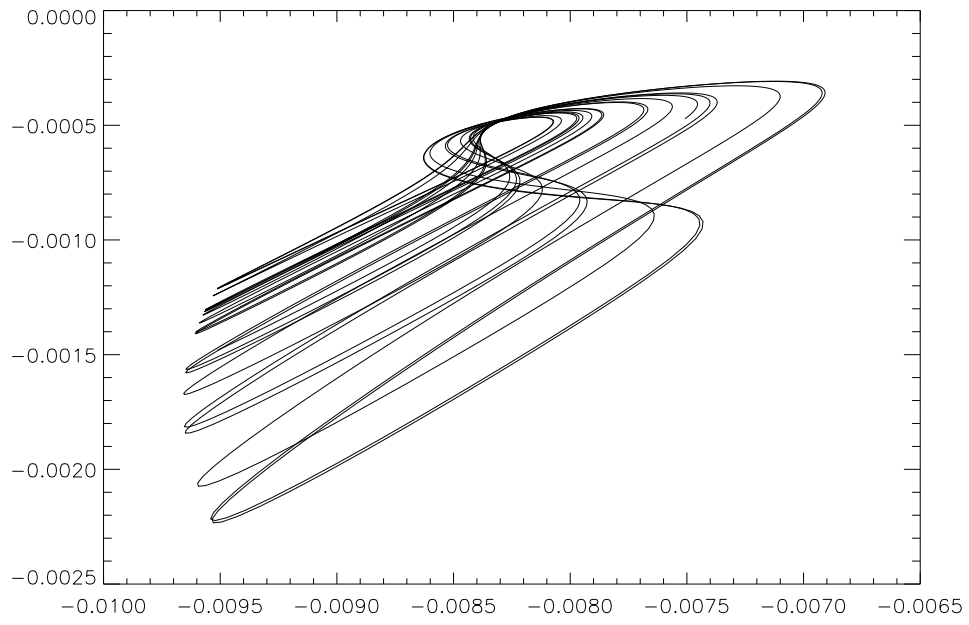


Figure 3c. Projection of the trajectory in the phase space in saturated regime (a periodic orbit  $P_{3,i}^\infty$ ) on the plane of Fourier coefficients  $\text{Im } b_{0,1,2}^1$  (horizontal axis) and  $\text{Re } v_{0,1,2}^1$  (vertical axis) for  $R = 4$  and  $R_m = 39.5$ .

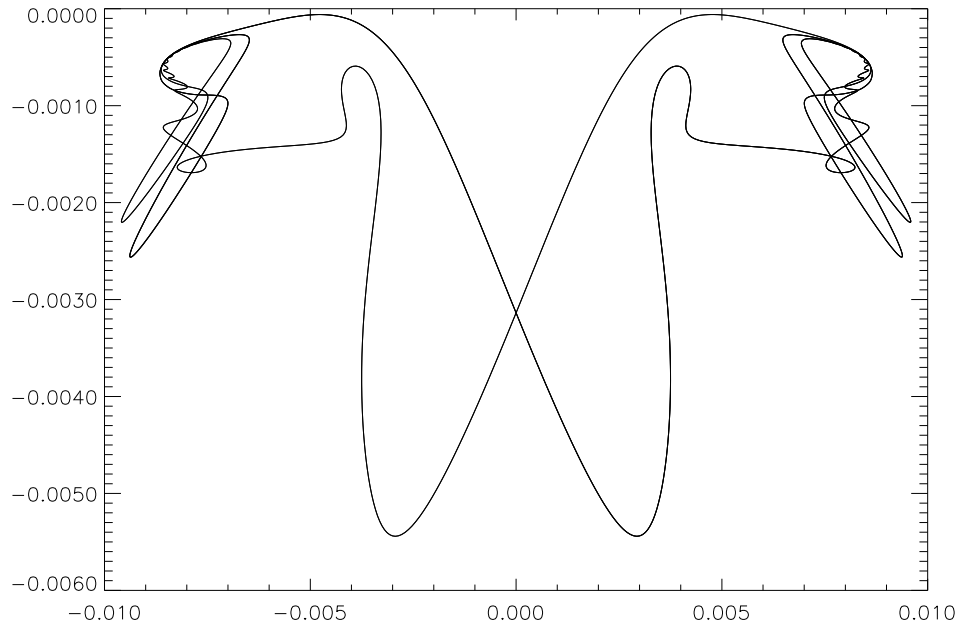


Figure 4a. Projection of the trajectory in saturated regime (periodic orbit  $P_4$ ) on the plane of Fourier coefficients  $\text{Im } b_{0,1,2}^1$  (horizontal axis) and  $\text{Re } v_{0,1,2}^1$  (vertical axis) for  $R = 4$  and  $R_m = 39.6$ .

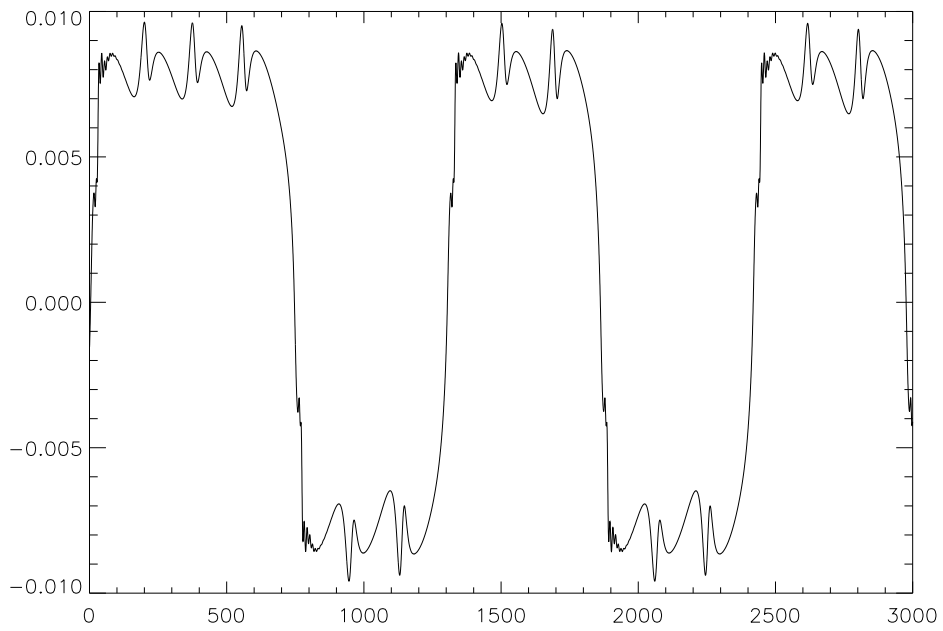


Figure 4b. Fourier coefficient  $\text{Im } b_{0,1,2}^1$  (vertical axis) as a function of time (horizontal axis) for  $R = 4$  and  $R_m = 39.6$  (same run as on Fig. 4a).

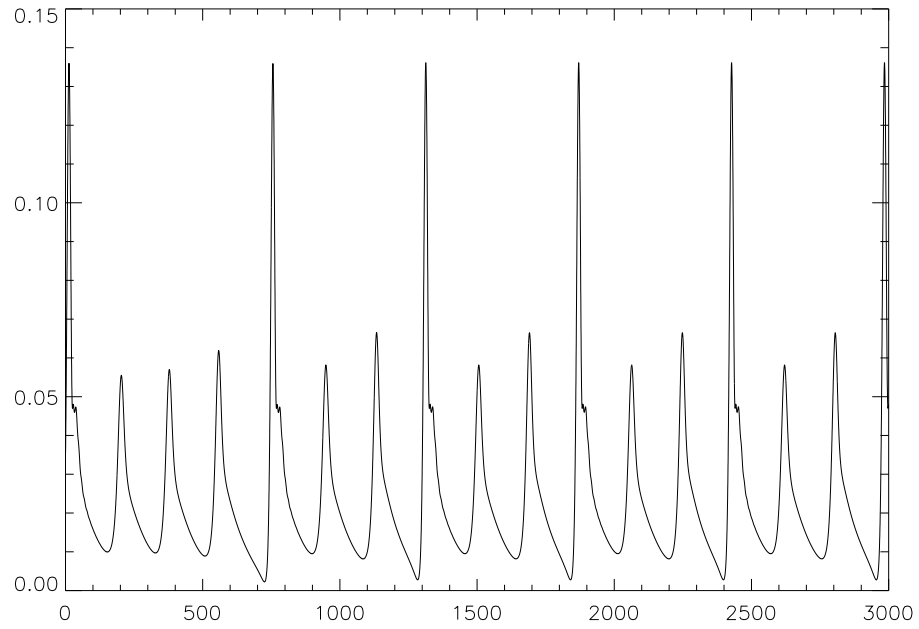


Figure 4c. Magnetic energy (vertical axis) versus time (horizontal axis) for  $R = 4$  and  $R_m = 39.6$  (same run as on Fig. 4a).

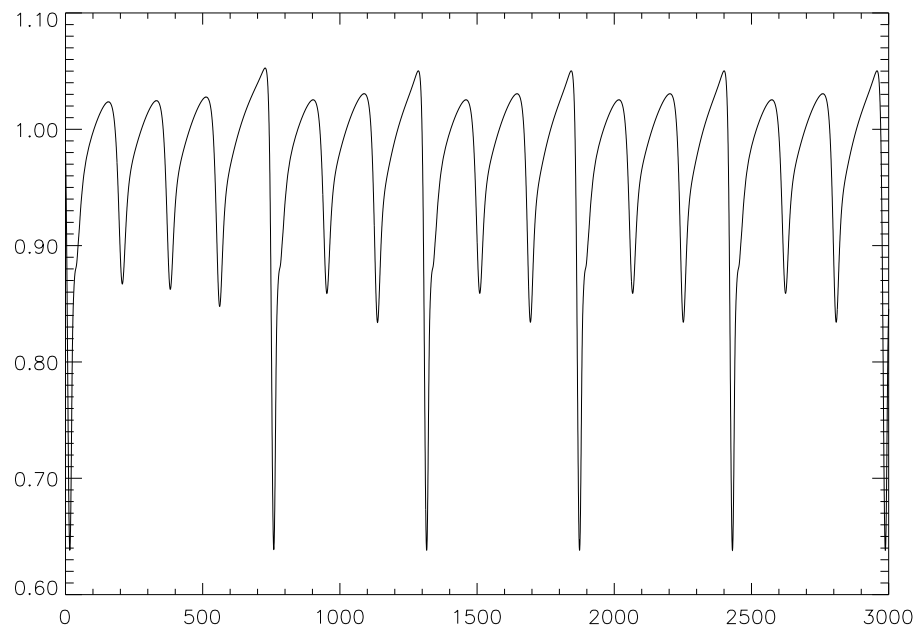


Figure 4d. Kinetic energy (vertical axis) versus time (horizontal axis) for  $R = 4$  and  $R_m = 39.6$  (same run as on Fig. 4a).

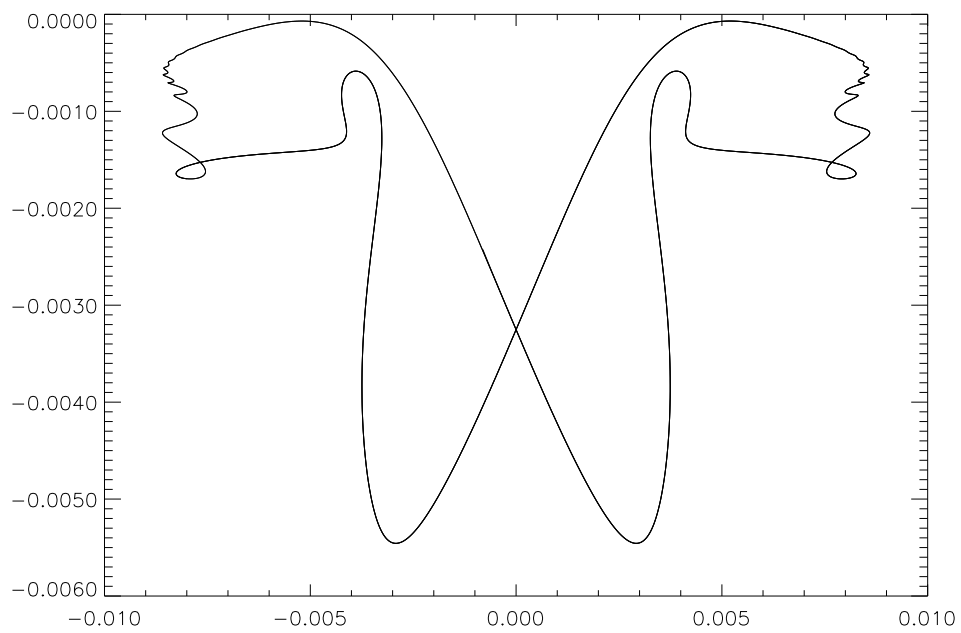


Figure 5. Projection of the trajectory in saturated regime (periodic orbit  $P_4$ ) on the plane of Fourier coefficients  $\text{Im } b_{0,1,2}^1$  (horizontal axis) and  $\text{Re } v_{0,1,2}^1$  (vertical axis) for  $R = 4$  and  $R_m = 39.7$ .

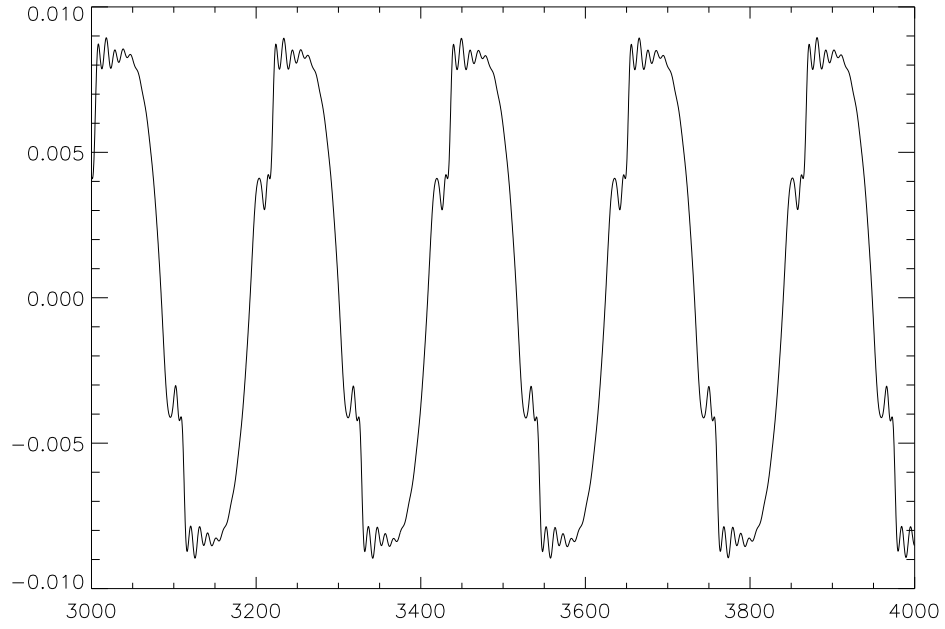


Figure 6a. Fourier coefficient  $\text{Im } b_{0,1,2}^1$  (vertical axis) as a function of time (horizontal axis) for  $R = 4$  and  $R_m = 42$ .

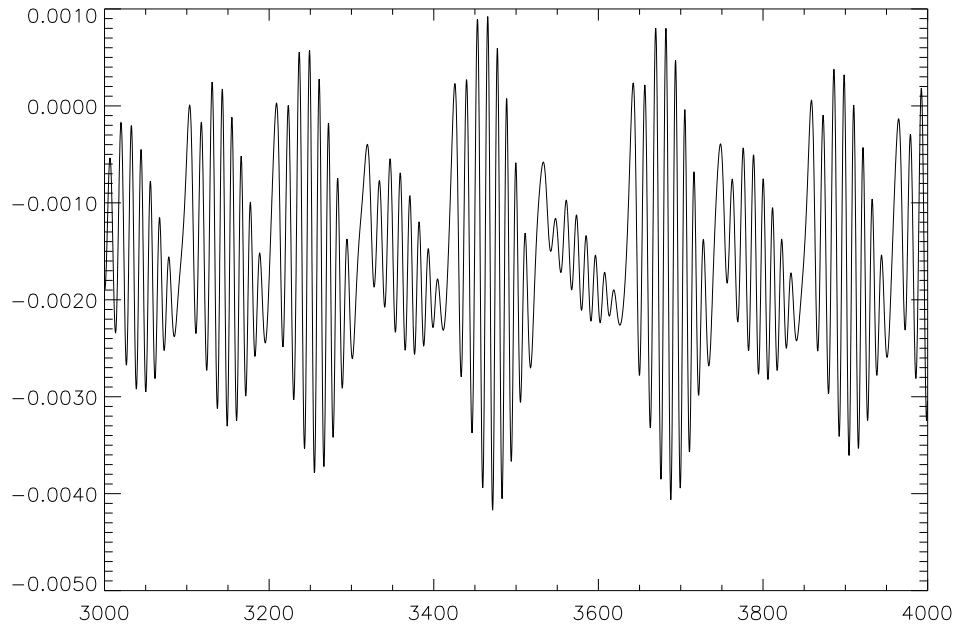


Figure 6b. Fourier coefficient  $\text{Re } b_{0,1,1}^3$  (vertical axis) as a function of time (horizontal axis) for  $R = 4$  and  $R_m = 42$  (same run as on Fig. 6a).

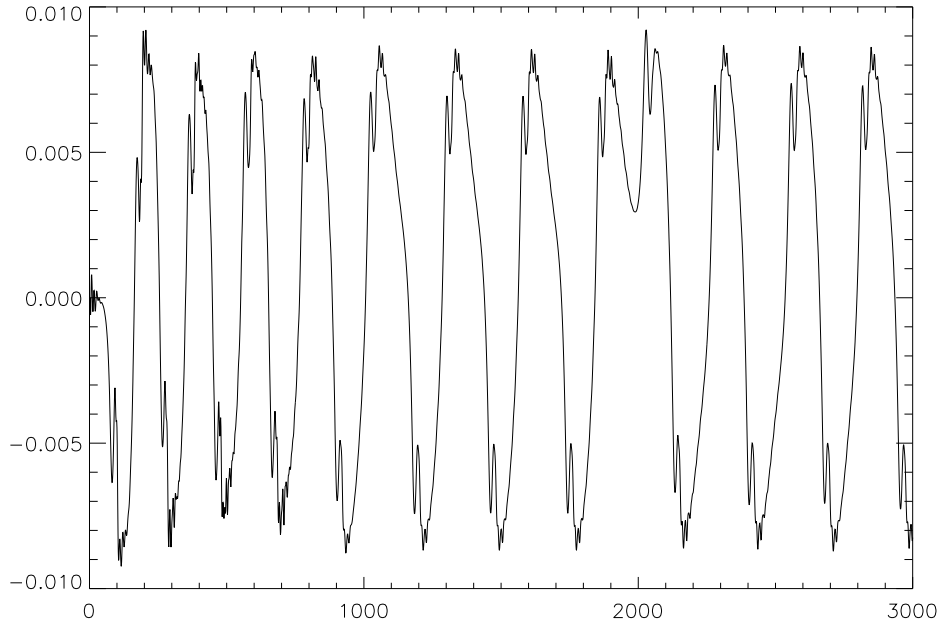


Figure 7a. Fourier coefficient  $\text{Im } b_{0,1,2}^1$  (vertical axis) as a function of time (horizontal axis) for  $R = 4$  and  $R_m = 45$ .

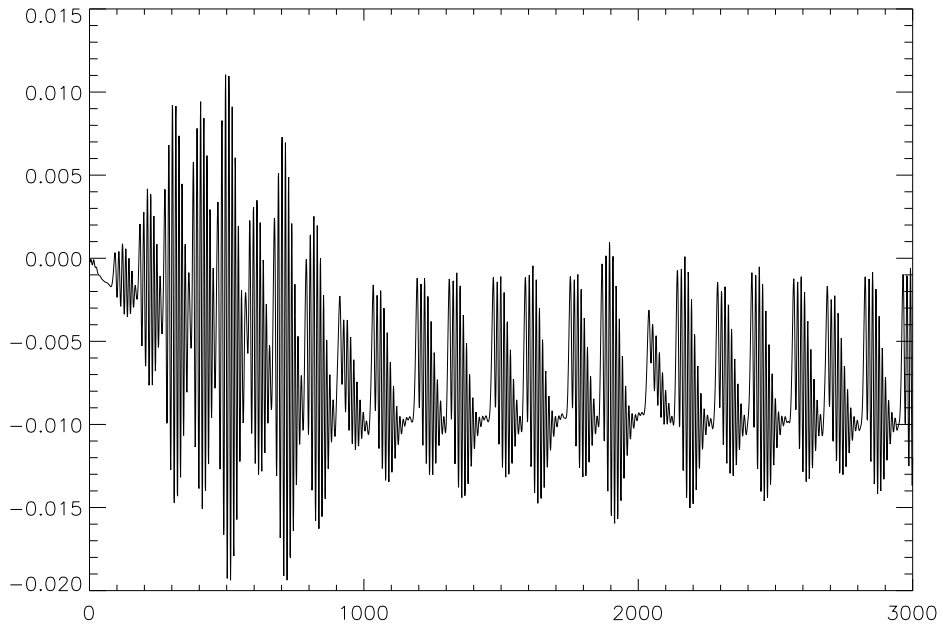


Figure 7b. Fourier coefficient  $\text{Re } b_{0,1,1}^3$  (vertical axis) as a function of time (horizontal axis) for  $R = 4$  and  $R_m = 45$  (same run as on Fig. 7a).

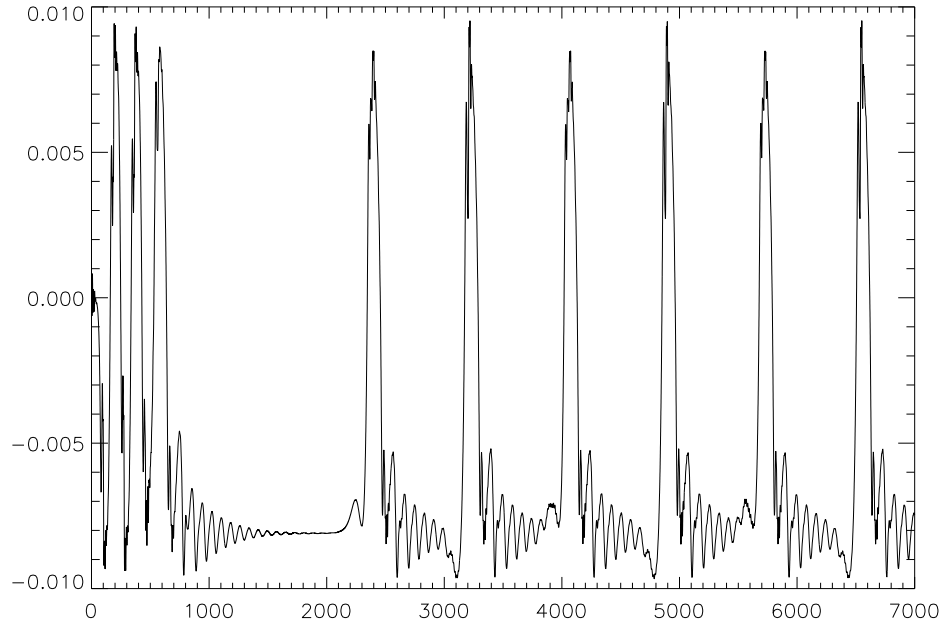


Figure 8a. Fourier coefficient  $\text{Im } b_{0,1,2}^1$  (vertical axis) as a function of time (horizontal axis) for  $R = 4$  and  $R_m = 46$ .

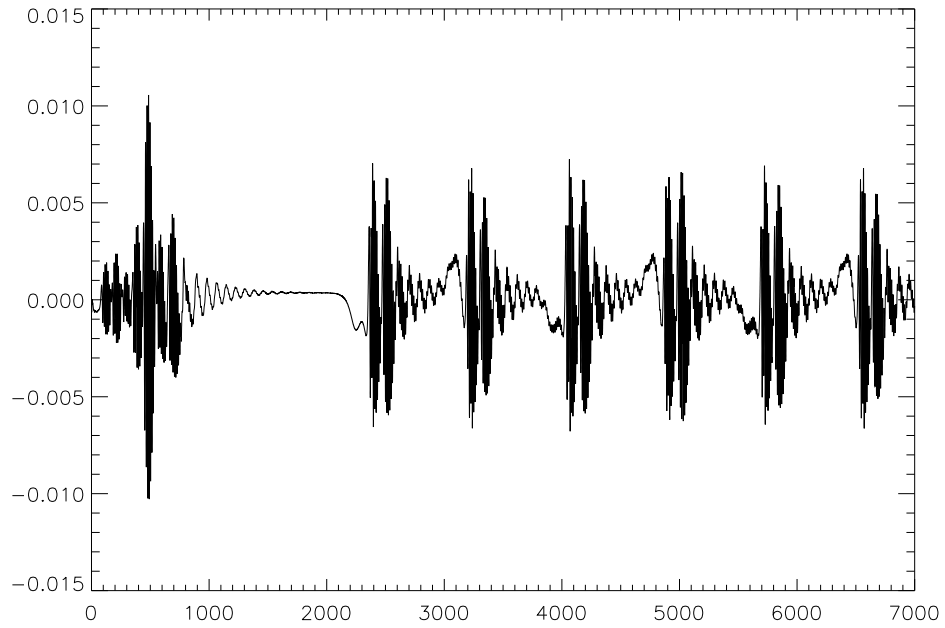


Figure 8b. Fourier coefficient  $\text{Re } b_{0,1,1}^3$  (vertical axis) as a function of time (horizontal axis) for  $R = 4$  and  $R_m = 46$  (same run as on Fig. 8a).

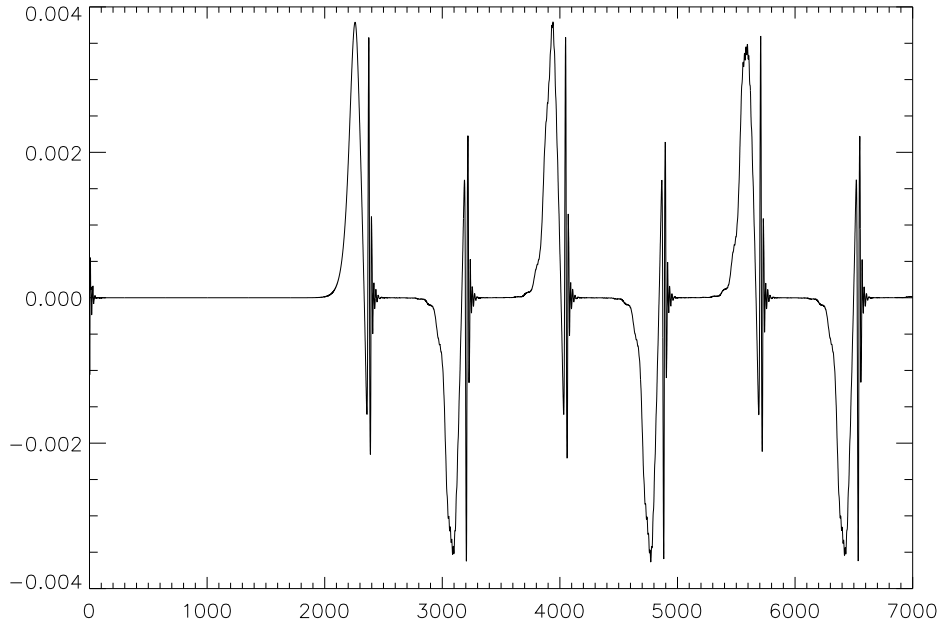


Figure 8c. Fourier coefficient  $\text{Re } b_{1,0,1}^3$  (vertical axis) as a function of time (horizontal axis) for  $R = 4$  and  $R_m = 46$  (same run as on Fig. 8a).

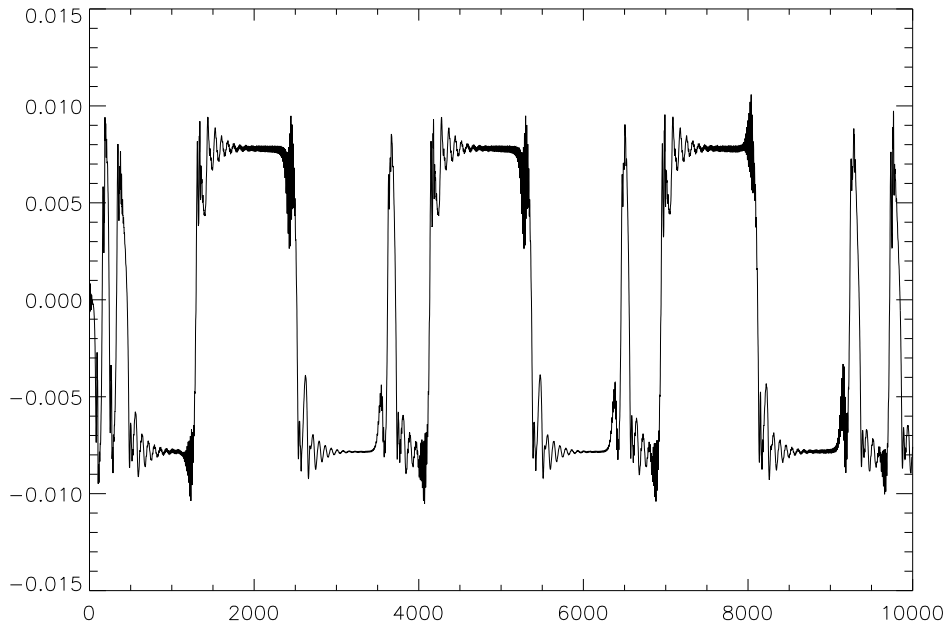


Figure 9. Fourier coefficient  $\text{Im } b_{0,1,2}^1$  (vertical axis) as a function of time (horizontal axis) for  $R = 4$  and  $R_m = 48$ .

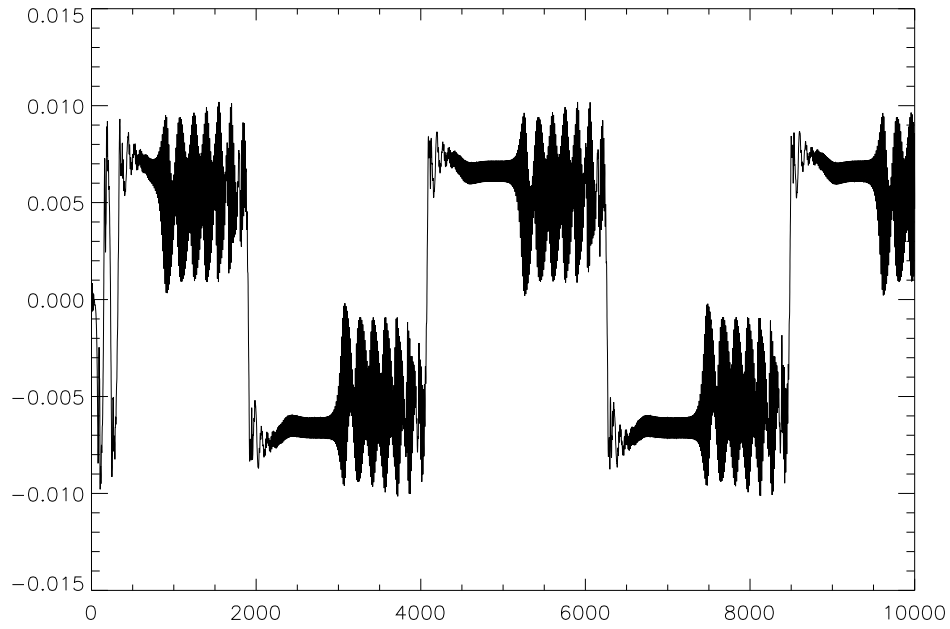


Figure 10a. Fourier coefficients  $\text{Im } b_{0,1,2}^1$  (vertical axis) as a function of time (horizontal axis) for  $R = 4$  and  $R_m = 51$ .

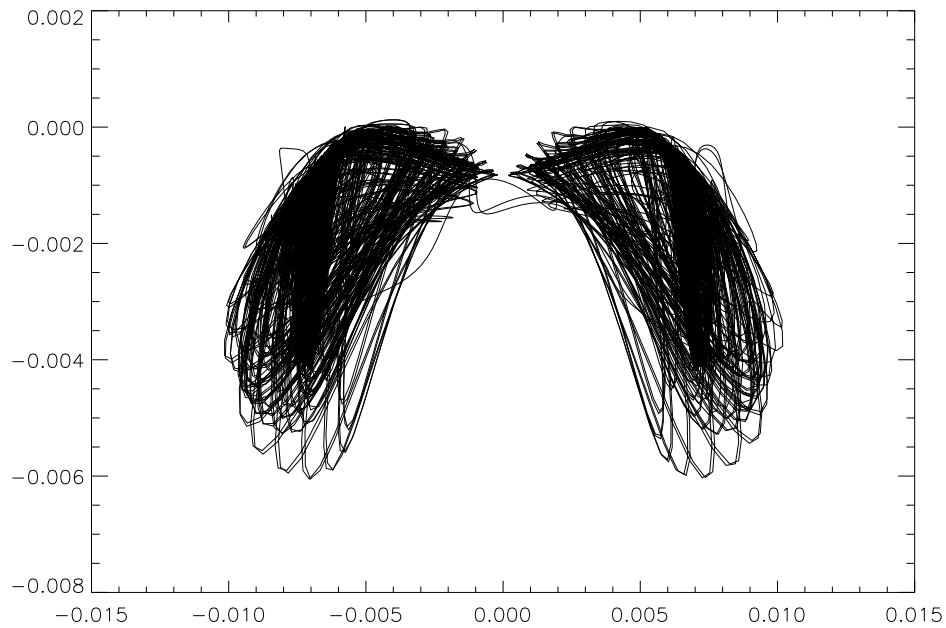


Figure 10b. Projection of the trajectory in saturated regime on the plane of Fourier coefficients  $\text{Im } b_{0,1,2}^1$  (horizontal axis) and  $\text{Re } v_{0,1,2}^1$  (vertical axis) for  $R = 4$  and  $R_m = 51$  (same run as on Fig. 10a).

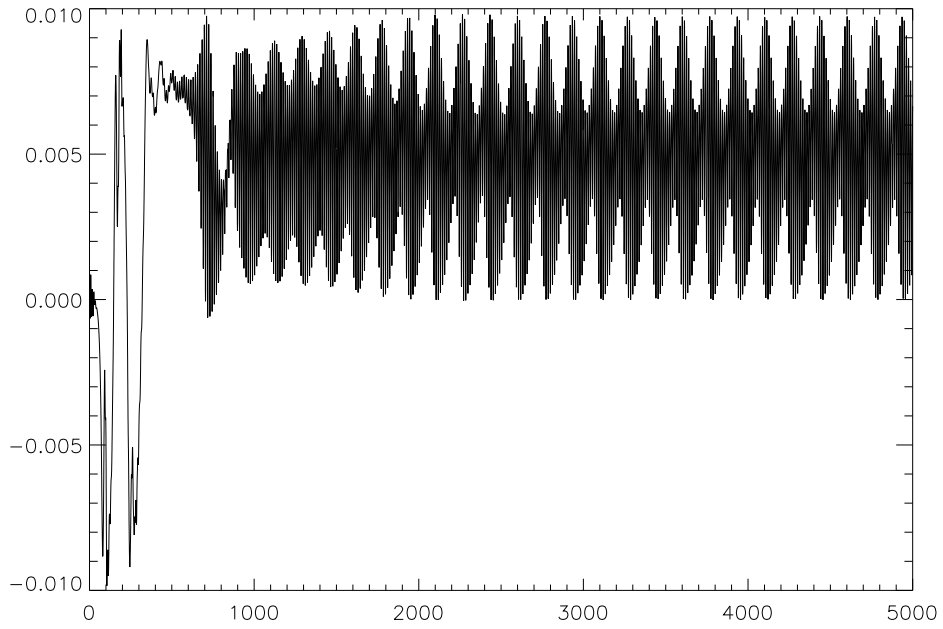


Figure 11a. Fourier coefficient  $\text{Im } b_{0,1,2}^1$  (vertical axis) as a function of time (horizontal axis) for  $R = 4$  and  $R_m = 52$ .

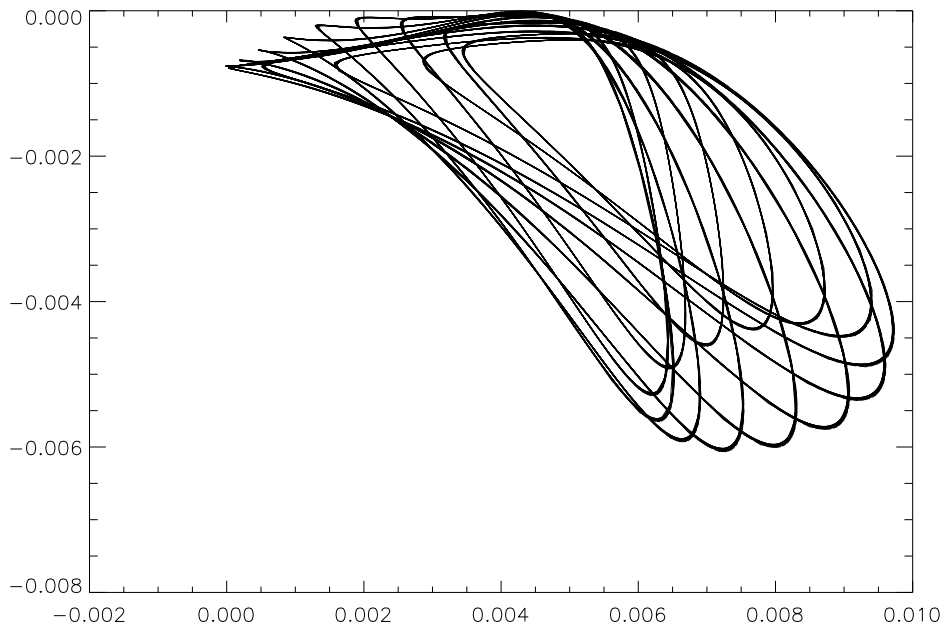


Figure 11b. Projection of the trajectory in saturated regime (torus  $T_{3,i}$ ) on the plane of Fourier coefficients  $\text{Im } b_{0,1,2}^1$  (horizontal axis) and  $\text{Re } v_{0,1,2}^1$  (vertical axis) for  $R = 4$  and  $R_m = 52$  (same run as on Fig. 11a).

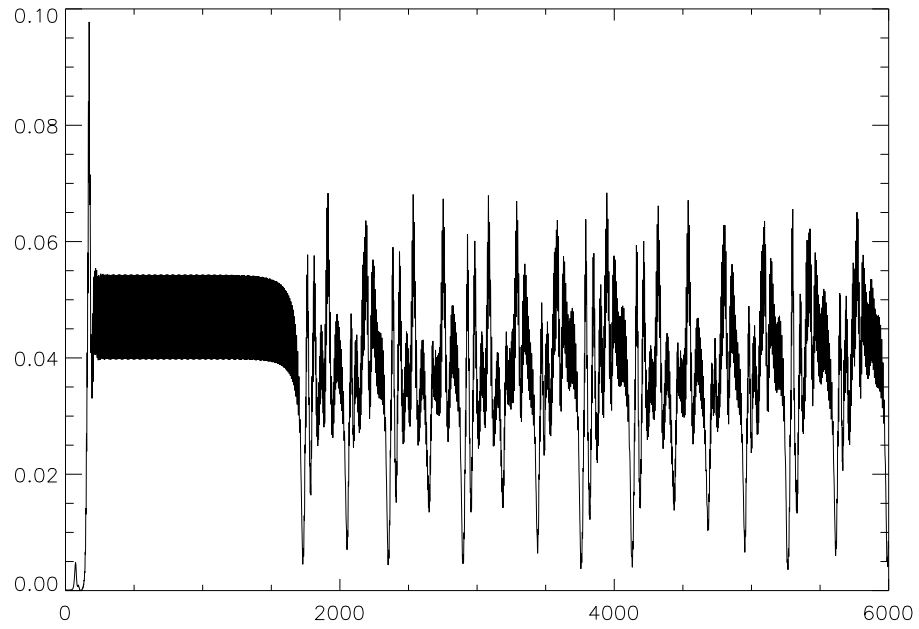


Figure 12. Magnetic energy (vertical axis) as a function of time (horizontal axis) for  $R = 15$  and  $R_m = 40$ .

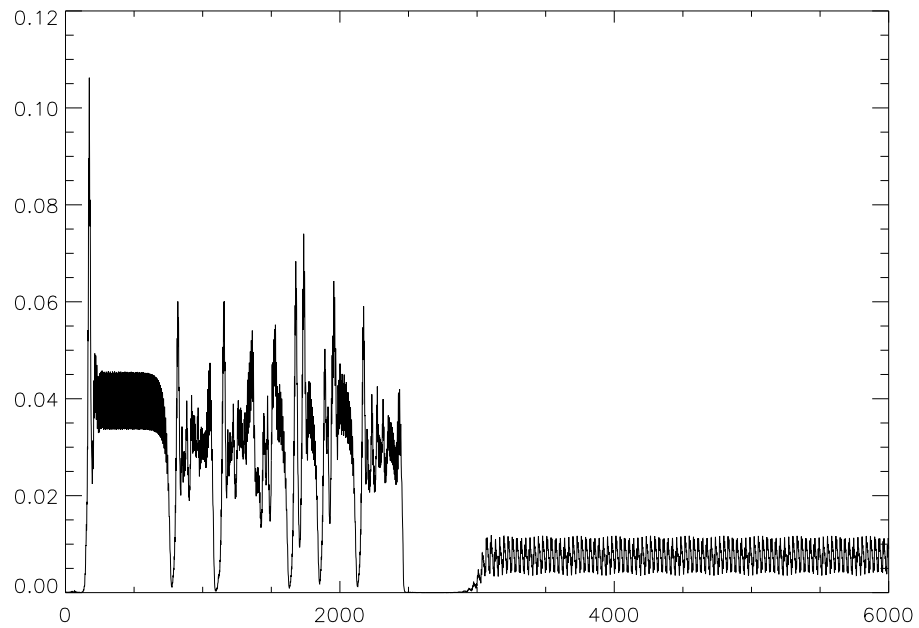


Figure 13. Magnetic energy (vertical axis) as a function of time (horizontal axis) for  $R = 20$  and  $R_m = 40$ .

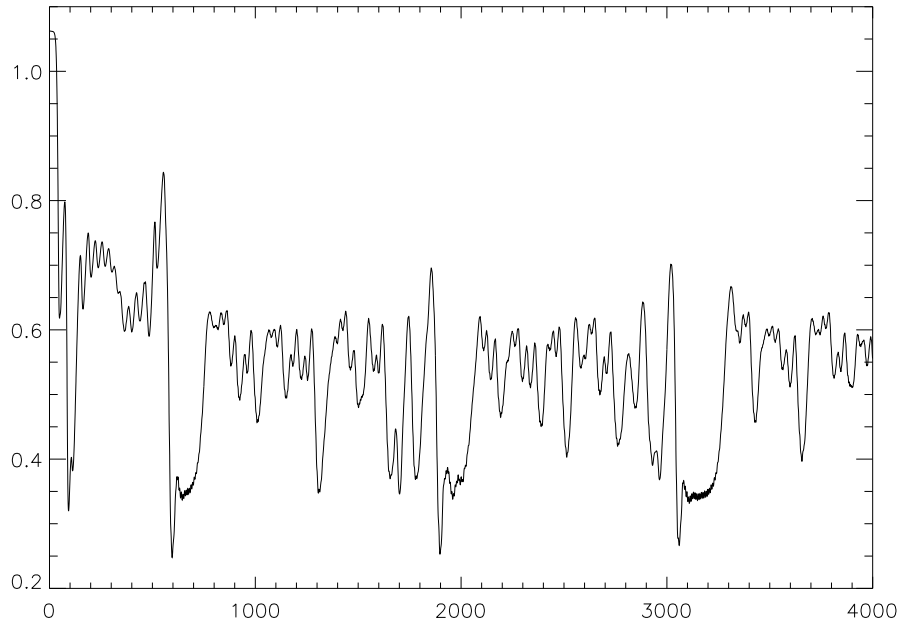


Figure 14a. Kinetic energy (vertical axis) as a function of time (horizontal axis) for  $R = 25$  and  $R_m = 40$ .

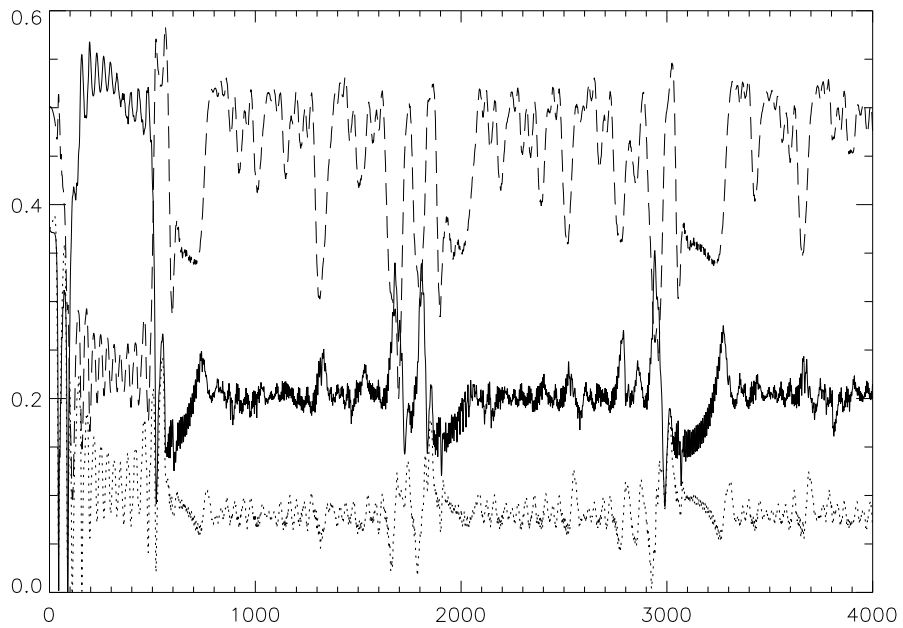


Figure 14b. Fourier coefficients of the flow (vertical axis: solid line –  $\text{Re } v_{1,0,0}^3$ , dashed line –  $\text{Re } v_{0,1,0}^1$ , dot line –  $\text{Re } v_{0,0,1}^2$ ) as a function of time (horizontal axis) for  $R = 25$  and  $R_m = 40$  (same run as on Fig. 14a).

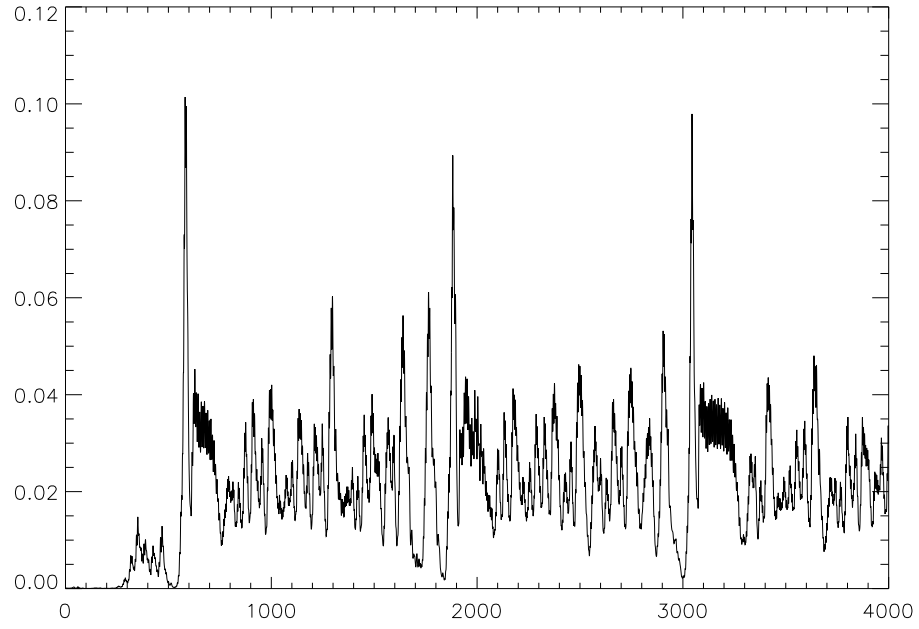


Figure 14c. Magnetic energy (vertical axis) as a function of time (horizontal axis) for  $R = 25$  and  $R_m = 40$  (same run as on Fig. 14a).

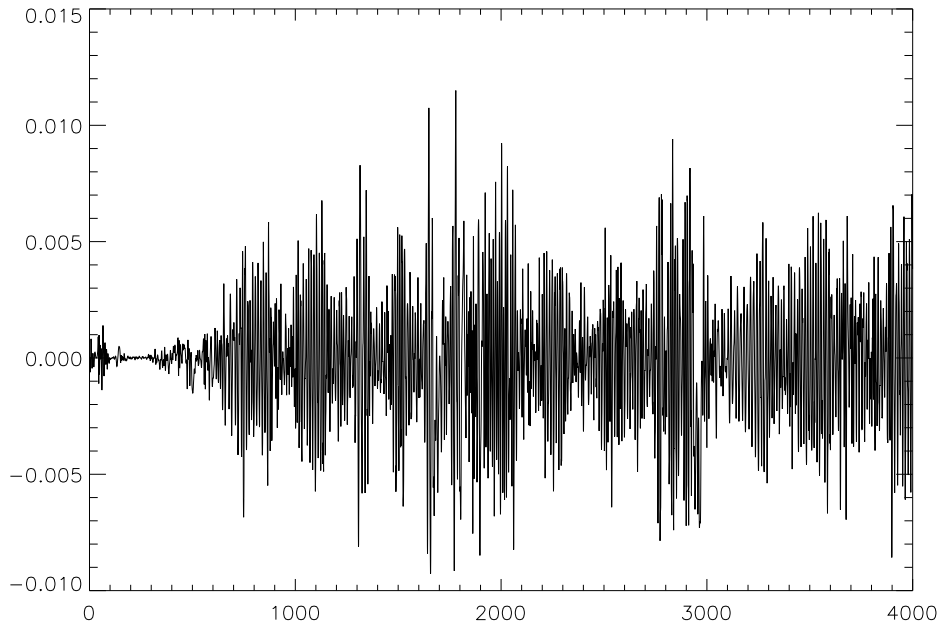


Figure 14d. Fourier coefficient  $\text{Im } b_{0,1,2}^1$  (vertical axis) as a function of time (horizontal axis) for  $R = 25$  and  $R_m = 40$  (same run as on Fig. 14a).

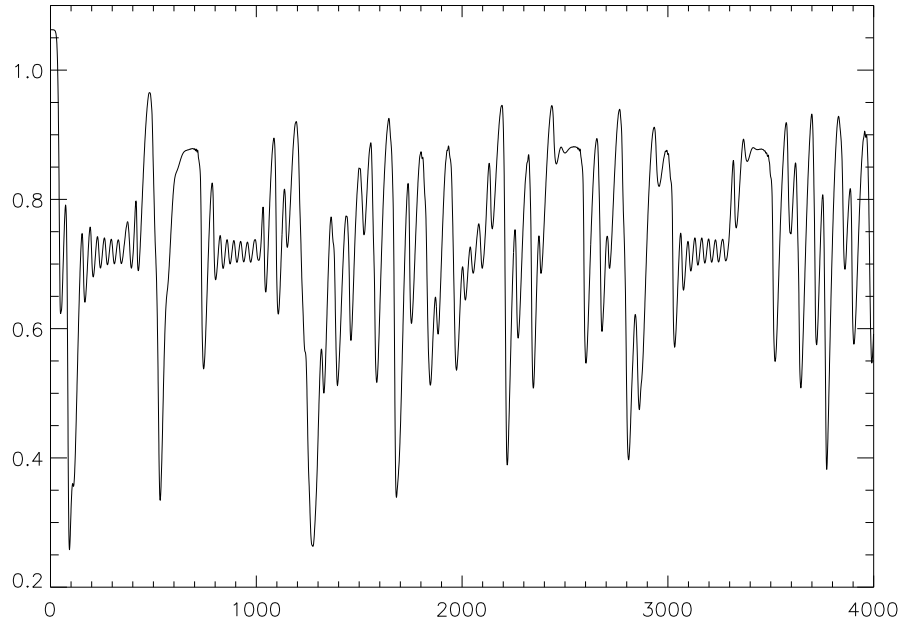


Figure 15a. Kinetic energy (vertical axis) as a function of time (horizontal axis) for  $R = 25$  in the hydrodynamic problem (the initial condition for the flow is the same as on Fig. 14).

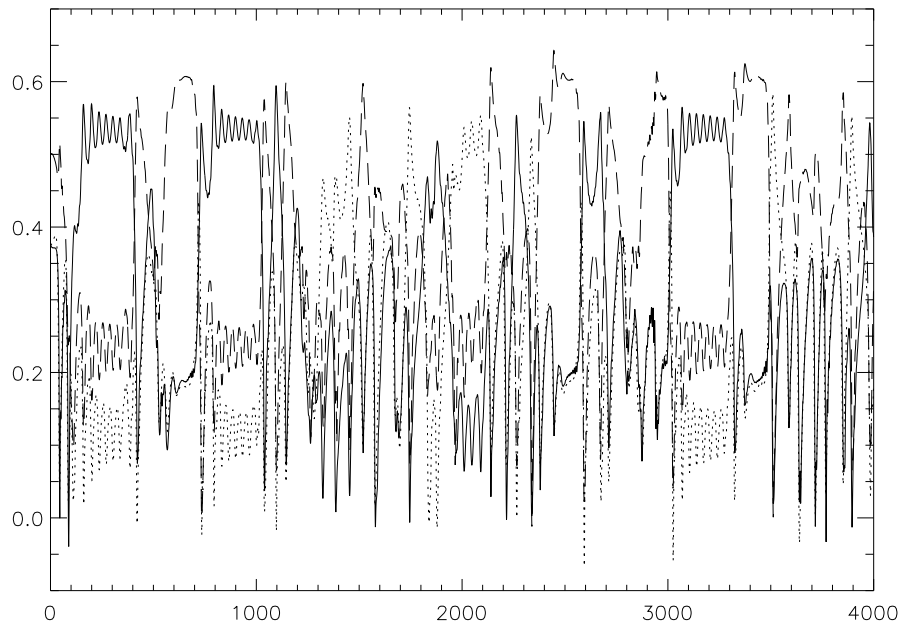


Figure 15b. Fourier coefficients of the flow (vertical axis: solid line –  $\text{Re } v_{1,0,0}^3$ , dashed line –  $\text{Re } v_{0,1,0}^1$ , dot line –  $\text{Re } v_{0,0,1}^2$ ) as a function of time (horizontal axis) for  $R = 25$  (same run as on Fig. 15a).

